Exp Fluids (2012) 53:1233–1250
DOI 10.1007/s00348-012-1356-7

RESEARCH ARTICLE

Scale effect on unsteady cloud cavitation

M. Dular · I. Khlifa · S. Fuzier · M. Adama Maiga · O. Coutier-Delgosha

Received: 18 December 2011 / Revised: 29 June 2012 / Accepted: 19 July 2012 / Published online: 9 August 2012

Abstract No experiment was conducted, yet, to investigate the scale effects on the dynamics of developed cavitating flow with periodical cloud shedding. The present study was motivated by the unclear results obtained from the experiments in a Venturi-type section that was scaled down 10 times for the purpose of measurements by ultrafast X-ray imaging (Coutier-Delgosha et al. 2009). Cavitation in the original size scale section (Stutz and Reboud in Exp Fluids 23:191–198, 1997, Exp Fluids 29:545–552 2000) always displays unsteady cloud separation. However, when the geometry was scaled down, the cavitation became quasi steady although some oscillations still existed. To investigate this phenomenon more in detail, experiments were conducted in six geometrically similar Venturi test sections where either width or height or both were scaled. Various types of instabilities are obtained, from simple oscillations of the sheet cavity length to large vapor cloud shedding when the size of the test section is increased. It confirms that small scale has a significant influence on cavitation. Especially the height of the test section plays a major role in the dynamics of the re-entrant jet that drives the periodical shedding observed at large scale. Results suggest that the sheet cavity becomes stabile when the section is scaled down to a certain point because re-entrant jet cannot fully develop.

M. Dular
Laboratory for Water and Turbine Machines,
University of Ljubljana, Askerceva 6, 1000 Ljubljana, Slovenia

I. Khlifa · S. Fuzier · M. Adama Maiga ·
O. Coutier-Delgosha (✉)
Laboratoire de Mécanique de Lille (LML)/Arts et Metiers
ParisTech, 8 Boulevard Louis XIV, 59046 Lille, France
e-mail: olivier.coutier@lille.ensam.fr

1 Introduction

Many spurious effects of cavitation in rotating machineries are due to its unsteady character: the sheet cavities on the suction side of the blades are usually characterized by periodical or non-periodical large-scale oscillations, while the condensation areas are submitted to complex unsteady mechanisms involving high pressure fluctuations. This dynamics is responsible for phenomena such as vibrations, noise, erosion of solid surfaces, increase of hydrodynamic drag, and large pressure fluctuations that may be prejudicial for the other components of the machinery. To avoid or at least to reduce such effects of cavitation by design and operation measures, there is a persistent need of improving the understanding of the physical phenomena underlying the harmful effects.

Therefore, unsteady cavitation is studied in cavitation tunnels in configurations of simple geometries such as two-dimensional (2D) foil sections or Venturi-type sections, in order to improve the knowledge about the structure of the two-phase flow and the mechanisms that control its unsteady features (see for example Furness and Hutton 1975; Stutz and Reboud 1997, 2000; Arndt et al. 2000; Laberteaux and Ceccio 2001a, b; Dular et al. 2004; Coutier-Delgosha et al. 2007). Various scales of the samples have been used in previous studies, varying usually between a few centimeters (Pham et al. 1999; Stutz and Reboud 1997) and a few meters (Park et al. 2003).

In such flow configurations, cloud cavitation usually leads to Strouhal numbers $St = f \times L_{cav}/V_{ref}$ close to 0.25/0.3, where f is the oscillation frequency of the sheet cavity, L_{cav} is the mean cavity length, and V_{ref} a reference velocity usually considered upstream from the cavitation area. Lower values of St have also been found in a case of cavitation on 2D foil sections, for hydrodynamic conditions

resulting in a parameter $\sigma/2\alpha < 4$ (Arndt et al. 2000) where σ and α denote the cavitation number and the foil incidence, respectively. Further investigations have shown that such slow down of the periodical behavior is obtained for example in flow configurations involving an interaction with a pressure side cavity (Coutier-Delgosha et al. 2007) or the influence of the pressure wave due to the collapse of the vapor cloud for particular incidence angles of a 2D NACA profile (Leroux et al. 2005).

Influence of the sample scale on the dynamics of cloud cavitation and the value of the Strouhal number has not been investigated, yet, although the occurrence of scale effects on cavitation has long been known and was already mentioned by Ackeret (1930). In the 1970s, comparative tests on hydrofoils were performed in the scope of a test program whose objective was to determine the effects of flow velocity and water gas content on the inception of cavitation. The data showed large differences between the various tunnels and observers (Callejon et al. 1978). In addition, numerous studies of scaling laws in cavitating flow were performed, but they all dealt with the problem of cavitation occurrence, while the case of fully developed cavitating flow was not considered (Holl et al. 1972; Arakeri and Acosta 1973; Gates and Billet 1980; Billet and Holl 1981; Ooi 1985; Amromin 2002).

In one of the best known and most thorough studies on scale effects, Keller (2001) showed that, provided effects of water quality are avoided in the experiments, very clear empirical relations can be established for the scale effects of tip vortex cavitation inception. He also indicated that the scaling relations, which would enable to predict the extent of the cavitation area, could also remain valid for developed cavitation and also for other types of cavitating flow, which are not dependant on the underlying vertical flow (surface cavitation on a 2D hydrofoil, cavitation on an arbitrary-shaped non-lift producing bodies). He, however, does not mention the problem of the scaling and the dynamics of cavitation.

Remarkably, no experiment was conducted, yet, to investigate the scale effects on the dynamics of developed cavitating flow with cloud shedding. The present study was motivated by the unclear results obtained from the experiments in a Venturi-type section with convergent and divergent angles of 18° and 8°, respectively (Coutier-Delgosha et al. 2005), which was scaled down 10 times (height 3.3 mm at the Venturi throat, width 4 mm) in order to perform measurements by ultra-fast X-ray imaging method (Vabre et al. 2009). Although the selected geometry should trigger vapor cloud shedding, results imply that the cavity is quasi-stabile (Coutier-Delgosha et al. 2009).

To understand the reason for this flow stabilization, six geometrically similar test sections were manufactured, and the cavitation dynamics was investigated in the six cases. In three sections, both the height h and the width b of the channel were scaled. In the three other ones, only one dimension was scaled in order to isolate the influence of the other dimension. For each section, nine hydraulic conditions, based on a combination of three flow velocities and three cavitation numbers, were tested. For evaluation of cavitation dynamics, high-speed imaging, conventional imaging, microphone measurements and accelerometer measurements were used.

The experimental setup is detailed in Sect. 2 of the paper, while Sect. 3 is devoted to the presentation of the results: characteristic frequencies, flow dynamics, and flow structure are successively compared in the six test sections. These data are discussed in Sect. 4.

2 Experimental setup

Experiments were conducted in the small cavitation tunnel VenturiX of the LML Laboratory (Lille, France). This tunnel was designed for the special purpose of velocimetry in a cavitating flow by ultra-fast X-ray imaging (Vabre et al. 2009). Its main specificity consists of a very small test section (width 4 mm and height close to 3 mm at the Venturi throat) that was designed in order (1) to enable detection of very small radio-opaque particles (diameter 17 μm), (2) to minimize the thickness of water and Plexiglas crossed by the X-rays, (3) to obtain a transportable test rig to perform the measurements in the Advanced Photon Source of the Argonne National Laboratory (USA). All details related to the conception of the cavitation tunnel can be found in Coutier-Delgosha et al. (2009).

2.1 Test rig

Figure 1 presents the organization of the test rig. Circulation of water is obtained with a Salmson Multi HE 403 pump (1) that enables the variation of the rotation speed between 0 and 3,600 rpm in order to set the mass flow rate. At the pump delivery, a tank completely filled with the circulation water (2) is used for water cooling in order to maintain a constant temperature close to 20 °C in the test rig. Cooling water flows inside the tank in a secondary loop (3) which is connected to cold (14 °C) tap water. Water temperature can also be increased with an immersion heater TCV020 of output 2,000 W (4). The volume flow rate is measured with two flow meters (5 and 6). The first one is a turbine flow meter Bürkert type 8032 (DN 6) whose uncertainty is 0.15 l/min after in situ calibration, and the second one is an electromagnetic flow meter Bürkert type 8045 (DN 15) with a 2 % uncertainty on measurements. The recorded values from the two devices did not differ for more than 1 %. Eventually an average

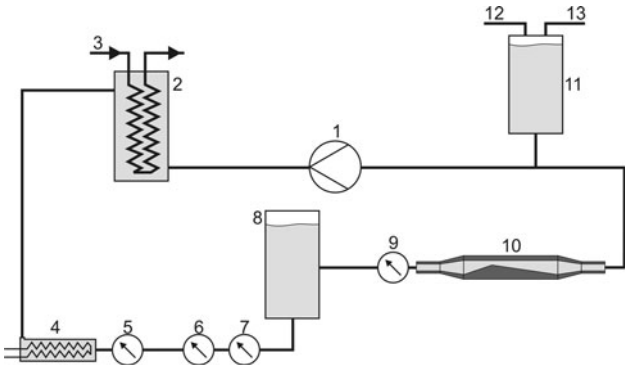

Fig. 1 Scheme of the test rig

value of the two measurements was used to calculate the mass flow rate and the reference velocity at the Venturi throat. Temperature is obtained with a type K thermocouple (7) which is directly in contact with the circulation water. Upstream from the test section (10), a second tank (8) partially filled with water is used to filter the flow rate and/or periodical pressure fluctuations due to the passage of the pump blades. The reference pressure is measured 200 mm upstream from the Venturi-type section with a Rosemount 3051 pressure sensor (9). The uncertainty of the measurements was close to 10 mbar. The pressure in the test rig is adjusted in the partially filled tank (11) connected to a compressor (12) and a vacuum pump (13), which enables to vary the pressure in this tank between 0.1 bar and 3.5 bar.

Flexible pipes with inner diameter of 1″ are used to connect these different devices. Since the volume of the test rig is small (about 15 liters), special care has to be taken to minimize the influence of water gas content and temperature variations. Using a vacuum pump, the system pressure was lowered, and the water in the test rig was let to rest over the night prior to the measurements. This was necessary to enable degassing what consequently minimized the tensile strength effects that can greatly influence the cavitation behavior (Iwai and Li 2003). The degassing procedure was the same for every set of experiments—this ensured that the ensemble of the cavitation nuclei that was left inside the loop was always the same; hence making the experiments repeatable. Also experiments dealt with developed cavitation which is less prone to influences from the nuclei size and number than the incipient cavitation.

The pressure (9) and the velocity V_{ref} at the Venturi throat are used as reference values to calculate the cavitation number:

$$\sigma = \frac{P_{\text{ref}} - P_{\text{vap}}}{1/2 \rho V_{\text{ref}}^2} \quad (1)$$

where P_{vap} is the vapor pressure at temperature T and ρ is the liquid density. Decreasing the cavitation number results in higher probability in cavitation occurrence or leads to an increase of the magnitude of the already present cavitation. The precisions of the pressure and velocity measurements result in a mean uncertainty of 3.5 % for the cavitation number.

2.2 Venturi-type sections

Six Venturi-type sections are used in the present study. They are characterized by different sizes, but they are all based on the same convergent and divergent angles of 18° and 8°, respectively. This is very close to the geometry used for previous experiments devoted to X-ray imaging (Coutier-Delgosha et al. 2009), which was derived from the Venturi shape used in previous experimental work in the LEGI laboratory (Stutz and Reboud 1997; Coutier-Delgosha et al. 2005), at scale 1/10.

The Venturi shapes and the side walls were manufactured out of transparent acrylic glass (Fig. 2), in order to enable visual observation of cavitation from all sides (front, back, top and bottom), although only front and top view were considered. Sections have standard 1/2″, 3/4″, or 1″ fittings for the connection with the test rig piping. The transition from the acrylic glass to the fitting is made out of epoxy resin and glass fiber. The sections (acrylic part) were about 300 mm long.

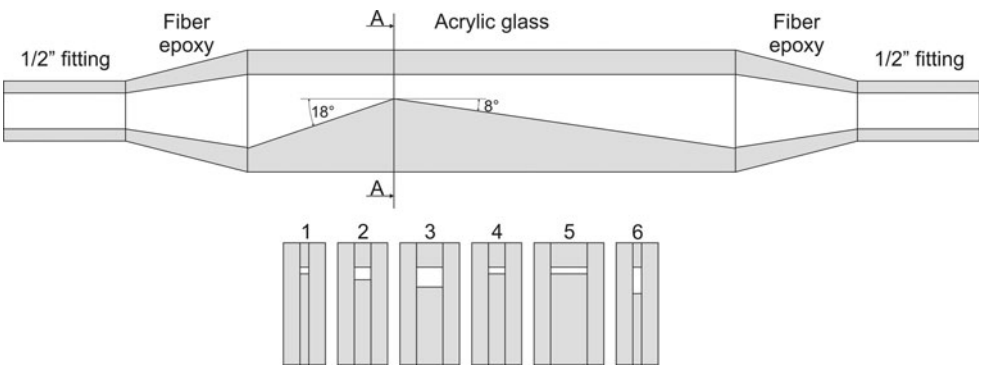

Fig. 2 Scheme of the six Venturi-type sections with cross-sections at the throat

Table 1 Dimensions of the test sections

Test section	Width (mm)	Height (mm)	Throat area (mm^2)	Scale
LEGI	44	33	1,452	1
X-ray experiments	4	3.3	13.2	1/10
TS1	3.6	2.7	9.7	1/12
TS2	6.8	5.1	34.7	1/6
TS3	10.8	8.1	87.5	1/4
TS4	6.8	2.7	18.4	–
TS5	15	2.7	40.5	–
TS6	3.6	10.8	38.9	–

The dimensions of the six sections are given in Table 1. For test sections TS1, TS2, and TS3, both the height h and the width b of the channel were scaled. Compared to the original dimensions of the test section in the LEGI laboratory, the present scales are about 1/12, 1/6, and 1/4, respectively. For sections TS4, TS5, and TS6, only one dimension (height or width at the throat) was scaled in order to isolate the influence of the other dimension.

Sections 1, 2 and 3 were used first to investigate in general whether the size of the throat of the section has an influence on cavitation dynamics. Then, when the influence was clearly shown by these experiments, sections 4 and 5 were used to inspect the influence of the section width, while the height remained the same as in section 1. Finally, section 6 was used to carry out experiments that would show the influence of the height of the section, while the width remained the same as in section 1.

2.3 Investigated cavitation conditions

For each test section, nine hydrodynamic conditions were investigated (data set 1: combination of three velocities at the Venturi throat $V_{ref} = 9$ m/s, 13 m/s, and 17 m/s and three cavitation numbers $\sigma = 0.96$, 0.98, and 1.01). Table 2 presents an overview of the 54 resulting operating points that have been investigated. For each of them, four experiments have been conducted, based on high-speed visualization and image acquisition from side, from top and from perspective view, respectively. A total number of 216 records are thus included in data set 1. A special care has been taken in the setting of the pressure and flow rate in the experiments, in order to impose exactly the nine selected flow conditions. However, slight deviations have been detected a posteriori. Values of V_{ref} and σ indicated in Table 2 are derived from the averaging of the 72 records in which they are constant (6 test sections, 3 values of V_{ref} or σ and 4 experiments at given flow conditions). The standard deviations of the velocity and cavitation number measurements are 0.1 m/s and 0.007, respectively.

The average temperature, obtained from the whole 216 experiments, is 16.7 °C, with a standard deviation of 0.9 °C. So, no thermal effect is expected in this study.

The first value of velocity $V_{ref} = 9$ m/s is nearly identical to the one applied in the experiments performed previously at scale 1 in the LEGI laboratory (Stutz and Reboud 1997). However, the Reynolds number based on the hydraulic radius at the Venturi throat is obviously much lower in the present case: $Re = 3.6 \times 10^5$ at scale 1, while it varies between 2.5×10^4 and 8.7×10^4 at reduced scale, for $V_{ref} = 9$ m/s. To include in the present study the possible effect of the Reynolds number on the results, higher values of Re have been investigated in two special configurations: TS1 (scale 1/12) and TS3 (scale 1/4). In this second data set, the Reynolds number has been increased up to 8.9×10^4 (TS1) and 2.6×10^5 (TS3) for a single value of the cavitation number $\sigma = 0.96$ already included in data set 1 (see Table 3).

Influence of the cavity length on the results has been also investigated by decreasing the cavitation number down to 0.91 (TS1) and 0.94 (TS3) for various Reynolds numbers. This third set of experiments (see Table 4) was

Table 2 Data set 1: investigated cavitation conditions

Test	V_{ref} (m/s)	σ (–)	Re					
			TS1	TS2	TS3	TS4	TS5	TS6
A	9	0.96	2.52×10^4	4.41×10^4	8.71×10^4	2.93×10^4	3.48×10^4	4.44×10^4
B	9	0.98	2.52×10^4	4.41×10^4	8.48×10^4	2.93×10^4	3.48×10^4	4.44×10^4
C	9	1.01	2.52×10^4	4.41×10^4	8.71×10^4	2.93×10^4	3.48×10^4	4.44×10^4
D	13	0.96	3.69×10^4	6.46×10^4	1.12×10^5	4.34×10^4	5.20×10^4	6.15×10^4
E	13	0.98	3.79×10^4	6.46×10^4	1.09×10^5	4.34×10^4	5.20×10^4	6.15×10^4
F	13	1.01	3.79×10^4	6.46×10^4	1.09×10^5	4.34×10^4	5.34×10^4	6.15×10^4
G	17	0.96	5.00×10^4	8.73×10^4	1.80×10^5	5.74×10^4	7.92×10^4	8.09×10^4
H	17	0.98	5.00×10^4	8.73×10^4	1.63×10^5	5.74×10^4	6.67×10^4	8.09×10^4
I	17	1.01	5.00×10^4	8.73×10^4	2.22×10^5	5.74×10^4	6.84×10^4	8.52×10^4

Table 3 Data set 2: influence of the Reynolds number

TS1			TS3		
V_{ref}	Re	σ (–)	V_{ref}	Re	σ (–)
8.8	2.38×10^4	0.96	7.3	6.75×10^4	0.96
11.7	3.16×10^4	0.96	9.4	8.64×10^4	0.96
14.4	3.90×10^4	0.96	11.5	1.08×10^5	0.96
17.2	4.66×10^4	0.96	13.5	1.28×10^5	0.96
19.8	5.36×10^4	0.96	15.6	1.47×10^5	0.96
23.8	6.44×10^4	0.96	17.6	1.70×10^5	0.96
27.9	7.56×10^4	0.96	19.7	1.95×10^5	0.96
32.9	8.91×10^4	0.96	21.8	2.06×10^5	0.96
			23.7	2.46×10^5	0.96
			25.1	2.60×10^5	0.96

Table 4 Data set 3: influence of the sheet cavity length

TS1			TS3		
V_{ref}	Re	σ (–)	V_{ref}	Re	σ (–)
17.9	6.05×10^4	0.91	7.1	6.56×10^4	0.94
19.8	6.54×10^4	0.91	9.2	8.47×10^4	0.94
21.6	7.12×10^4	0.91	11.3	1.05×10^5	0.94
23.0	7.59×10^4	0.91	13.4	1.26×10^5	0.94
24.1	7.95×10^4	0.91	15.3	1.45×10^5	0.94
26.1	8.63×10^4	0.91	17.4	1.68×10^5	0.94
			19.4	1.92×10^5	0.94
			21.4	2.07×10^5	0.94
			23.3	2.37×10^5	0.94

motivated by the analysis of the two first sets of data and the subsequent discussion regarding the effects of small scale on the dynamics of cavitation.

2.4 Acquisition devices

A conventional low-speed CCD camera Marlin F-145 was used to capture images of cavitation from side (1), top (2) and perspective view (3) (Fig. 3). Eight-bit pictures with resolution 860 × 1,280 pixels were recorded. The illumination was provided by a stroboscopic light. These records enable to determine the characteristic size of the sheet cavity and also to investigate the variations of the internal structure of the cavitation area. For each flow condition, 100 images were recorded, which is sufficient for statistical evaluation later on (Dular et al. 2004).

To investigate the dynamics of cavitation, a high-speed camera Mikrotron Eosens mini1 was used. Images of cavitation structures were captured from the side view (see Fig. 3). The acquisition frequency was 3,000 fps at a resolution of 500 × 200 pixels in 8-bit resolution. Illumination was provided by a continuous light source. For each cavitation condition, 3,000 images (1 s) were recorded.

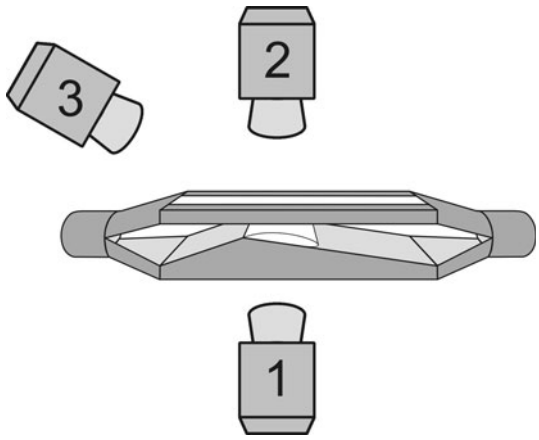

Fig. 3 Positions of the cameras: (*1*) side view, (*2*) top view, and (*3*) perspective view

In addition to flow visualization, the characteristic frequency of the two-phase flow fluctuations was also investigated by two other means: (1) a SONY ECM DM5P microphone (frequency range 100–15,000 Hz) located very close to the Venturi throat, (2) an accelerometer (Bruel and Kjaer, type 4375, voltage sensitivity 5.85 mV/g) fixed on a side wall of the test section, at the approximate location of the sheet cavity. Both signals were recorded simultaneously at frequency 8,000 Hz and analyzed by fast Fourier transform (FFT) in order to detect possible periodical sheddings and/or sheet cavity oscillations.

2.5 Evaluation techniques

Mean values and standard deviations of the gray level of images were calculated for the purpose of evaluation of mean cavity length and location of cloud separation, in case of unsteady behavior. This method was proposed in a previous paper by the present author (Dular et al. 2004) in order to get an objective determination of the mean characteristics and oscillation frequencies of the cavitation area. It was shown in this former study that the mean value and standard deviation of gray level in the images do not change significantly (less than 2 %) when taking in account more than 50 images.

To determine the frequency of the sheet cavity oscillations (or possible cavitation cloud shedding), power spectral density function (PSD) was calculated by FFT. As time series vector for the FFT, first a region of interest (ROI) was selected in the images. To exclude subjective choice of the position of ROI, a 50 × 50 pixels big region was selected with its center at the position of the maximum of the standard deviation of gray level—it was found by the

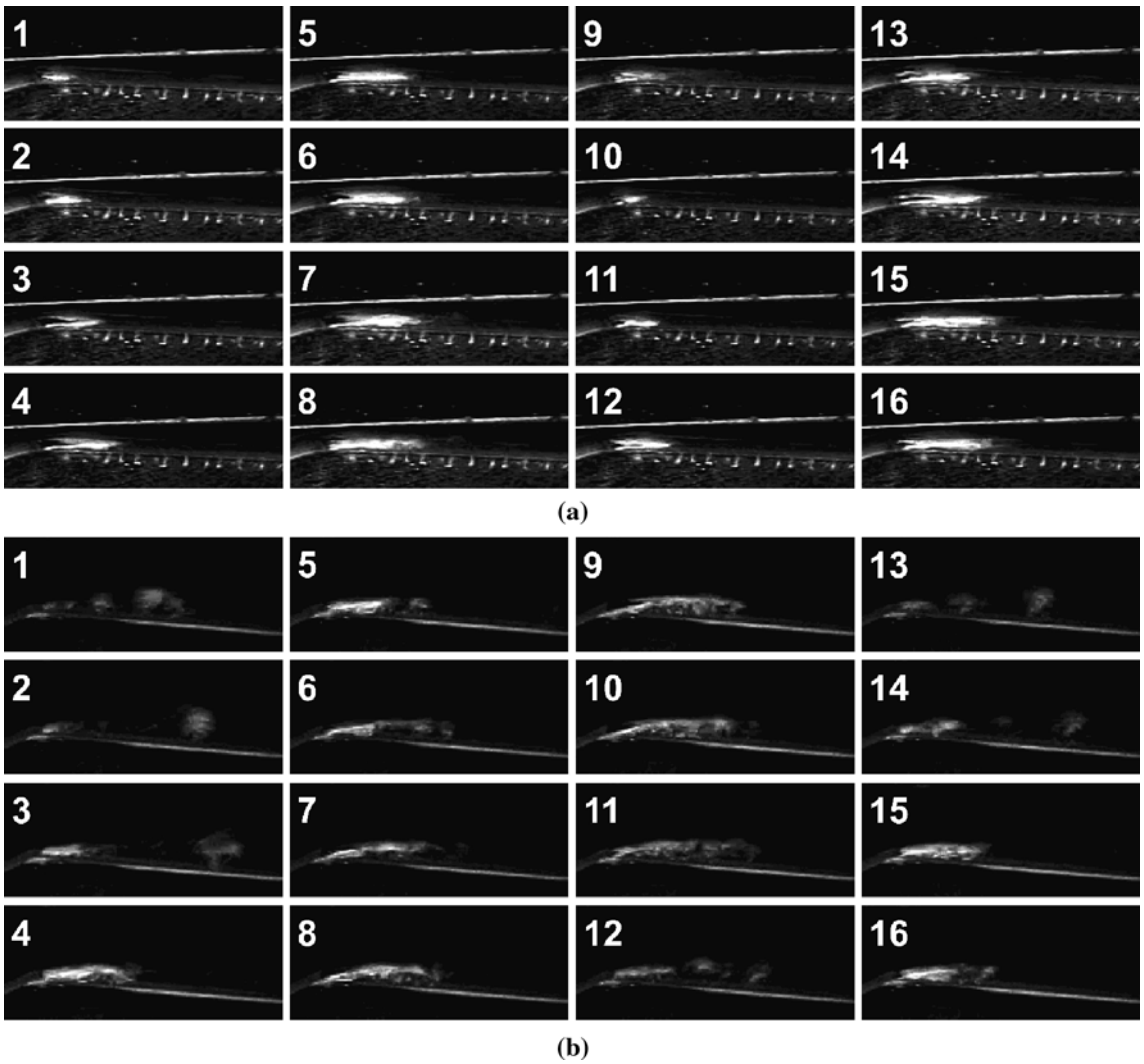

Fig. 4 Typical sequence for case A of data set 1 **a** with TS4 (no cloud shedding occurs) ($V_{ref} = 9$ m/s, $\sigma = 0.96$, $Re = 2.93 \times 10^4$), **b** with TS6 (cloud shedding) ($V_{ref} = 9$ m/s, $\sigma = 0.96$, $Re = 4.44 \times 10^4$)

present author (Dular et al. 2004) that the position of the maximum of the standard deviation of gray level correlates well with the position of maximal cavitation structure oscillation. For each vector element, the sum of the gray-level values of the 2,500 pixels included in this region of interest was used. For each flow condition, the duration of the record was 1 s, so the length of the time series vector was 3,000 elements. For each vector element, the sum of the gray-level values of the 2,500 pixels included in this region of interest was used. For each flow condition, the duration of the record was 1 s, so the length of the time series vector was 3,000 elements.

3 Results

A preliminary analysis of the recorded images reveals that the dynamics and the two-phase structure of cavitation differ from one test section to another. For example, Fig. 4a shows cavitation in TS4 for $\sigma = 0.96$ and $V_{ref} = 9$ m/s (measurement point A of data set 1). Figure 4b shows a sequence at the same operating point but in a bigger test section TS6. It can be observed that cavitation clouds are shed in TS6, while the attached cavity only oscillates without any shedding in TS4. These differences are detailed in the present section.

3.1 Non-dimensional mean length of the cavitation structure

The pixel intensity in images recorded in 8-bit resolution varies from 0 (black) up to 255 (white). Areas of cavitation look bright on the recorded images, so they are characterized by high values of gray level. The boundary of the cavitation structure in each image was defined as the isoline of gray level corresponding to 90 % of brightness. A

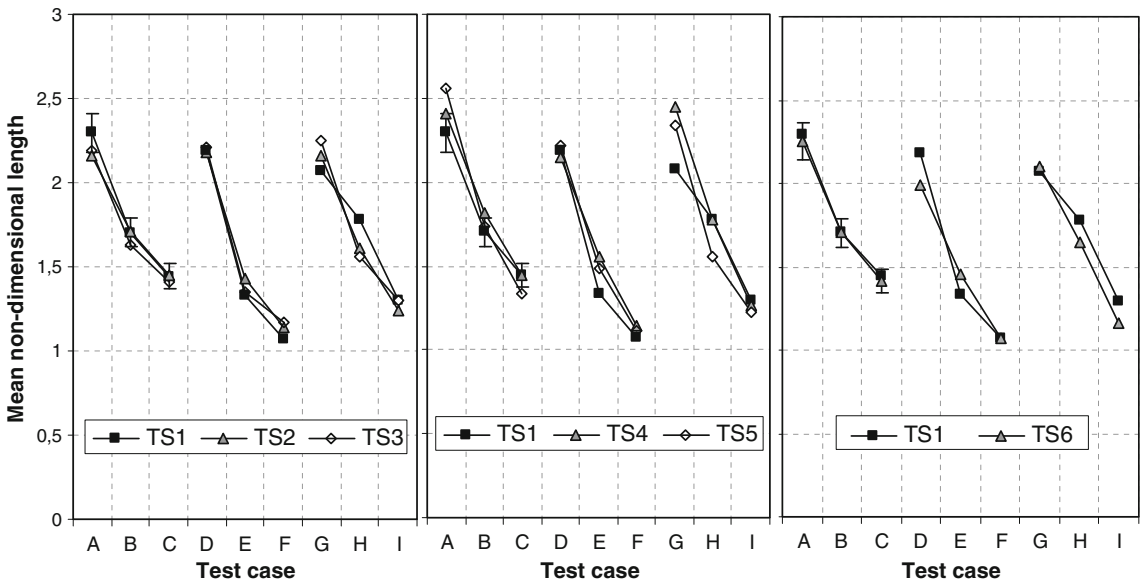

Fig. 5 Non-dimensional length of the averaged cavitation structures

time-averaged cavity shape was determined by averaging the sheet cavity boundary obtained from each image. Then, the mean length of the cavitation structure was derived for each flow configuration. Figure 5 consists of three diagrams that show the mean non-dimensional cavity length (mean cavity length divided by the channel height at the throat of the test section) for the 54 experiments of data set 1. Uncertainties on non-dimensional lengths, which are estimated to ±5 %, are indicated on some of the charts. The left diagram shows results for TS1, TS2, and TS3 where both dimensions of the Venturi section were scaled, the middle diagram shows the comparison where only the width was changed (TS1, TS4, TS5), and the right diagram shows the comparison where only the height of the section was increased (TS1 and TS6).

To investigate the influence of the test section size on the behavior of cavitation, the mean non-dimensional size of the cavity should be the same for all flow conditions based on the same cavitation number. This condition is required since the length of the cavitation area significantly influences its dynamics. It can be checked in Fig. 5 that this condition is fulfilled: the maximum disagreement between the non-dimensional lengths of sheet cavities at given cavitation number is close to 10 %, and it is usually much lower. These slight differences, which may be due to minor deviations of the pressure and the mass flow rate from the desired conditions, are small enough to include all operating points into the analysis hereafter.

3.2 Behavior of cavitation

Images from the high-speed records were observed to investigate the behavior of the two-phase flow. From the analysis of all flow conditions, four very distinctive behaviors were identified:

- Type 1: Cavitation clouds separate periodically from the attached part of cavitation, and they are convected by the main flow before collapsing downstream in a higher pressure region. A typical sequence can be seen in Fig. 4b. Such behavior is the one observed in the present configuration of Venturi-type section at large scale (see Stutz and Reboud 1997), with a Strouhal number based on the mean cavity length and the throat velocity close to 0.2. It has been much studied in various configurations of 2D foils and Venturi-type sections (Furness and Hutton 1975; Lush and Peters 1985; Pham et al. 1999; Arndt et al. 2000), and the large-scale cloud shedding is usually connected with the periodical re-entrant jet that flows upstream under the sheet cavity.
- Type 2: Single bubbles or small bubble clusters separate from the rear part of the sheet cavity. This behavior was obtained previously at larger scale in a configuration of Venturi with smaller angles (see Stutz and Reboud 1997) but never in the case of the present geometry.
- Type 3: The cavitation remains attached, but its size oscillates significantly (the length variations of the cavity are higher than 50 % of the mean cavity length during one period—usually about 75 %). A typical sequence can be seen in Fig. 4a.
- Type 4: The cavitation remains attached and the oscillations of its size are small (their amplitude is lower than 50 % of the mean cavity length during one period—usually about 25 %). A typical sequence can

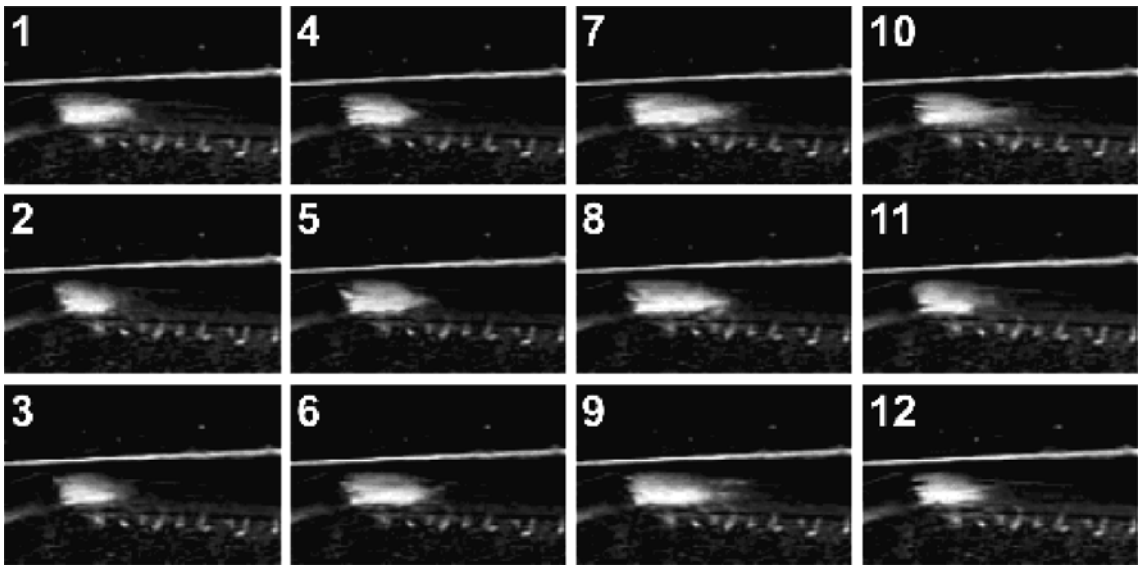

Fig. 6 Attached cavitation with small oscillations (TS4, case E of data set 1) ($V_{ref} = 13$ m/s, $\sigma = 0.98$, $Re = 4.34 \times 10^4$)

be seen in Fig. 6. Such behavior or the previous one is usually obtained at large scale only for very small sheet cavities.

In Table 5 are reported the types of cavitation for all hydrodynamic conditions. Unsteady behaviors including cloud shedding are found mainly with sections TS2, TS3, and TS6. On the other hand, almost no shedding (apart single bubbles from the rear part of the attached cavity) is obtained with TS1, while cavity detachment is observed in some cases only with TS4 and TS5 (highest velocities and/or biggest cavities). In most of the tests, behaviors with TS4 and TS5 belong to types 2, 3, or 4.

The first conclusion is that very small scale (TS1) leads to behaviors much different from the ones obtained at large scale: the sheet cavity oscillates without vapor detachment (types 3 or 4 in most of the cases), while periodical shedding is systematically observed at scale 1. This behavior is slightly modified with TS4 and TS5, which have the same throat height as TS1 but a bigger width: for cases A, B, or G, the sheet cavity shifts between cloud cavitation (type 1) and large oscillations of the attached cavity (type 3) which means that increasing the width of the test section has some effect on inception of cloud shedding. It can be postulated that increasing the width of the section reduces the effect of the side walls (and consequently the boundary layer effect), what enables another mechanism that triggers cavitation instability. However, for both test sections TS4 and TS5, the small height of the throat still does not allow undisturbed cavitation cloud shedding: type 1 is almost never obtained. Conversely, the classical unsteady behavior is recovered at larger scale with TS2 and TS3. It is also obtained with TS6 (small width, large height), which suggests that sufficient height of the throat is needed for undisturbed cavitation shedding.

It is also just to consider the influence of the throat area on the dynamics of cavitation. If one compares results in TS5 and TS6 which have a very similar throat area (40.5 and 38.9 mm^2, respectfully), yet very different geometry, one can see that the dynamics is significantly different. While type 1 cavitation is present in TS6, cavitation cloud shading rarely occurs in TS5, which has a small throat height. We can conclude that the dynamics is dependant on the geometry of the throat and not on its area. The same conclusion can be met also from an opposite point of view. We see from Table 5 that the cavitation in TS4 and TS5 displays very similar types of instabilities, yet the area of the throat is very different for these two test sections; the throat height, however, is the same.

3.3 Frequency of sheet cavity oscillations

Power spectral density function (PSD) based on local image analysis of the high-speed records was calculated to determine the characteristic frequency of sheet cavity oscillations. Frequencies equal to multiples of 50 Hz were all filtered in order to remove peaks due to brightness fluctuations of the continuous light source. On all spectra, low-frequency peaks related to the test rig influence can be observed. In addition, one or several big peaks are obtained at frequencies varying between 50 and 500 Hz, according to the test section and the flow conditions.

All these characteristic frequencies are reported in Table 6 for all test cases of data set 1. To analyze the data, a brief preliminary description of the spectra obtained with

Table 5 Type of unsteady cavitation instability

	Section 1	Section 2	Section 3	Section 4	Section 5	Section 6
A	2 and 3	1	1	2	1 and 3	1
B	3	1	1	2	1 and 3	1
C	4	1	1	4	4	1
D	3	1	1	2	2	1
E	4	1	1	2 and 4	2 and 4	1
F	4	1	1	4	4	1
G	4	1	1	1 and 3	1 and 3	1
H	4	1	1	2 and 4	2	1
I	4	3	1	4	4	1

Table 6 Frequency of sheet cavity oscillations

	Section 1	Section 2	Section 3	Section 4	Section 5	Section 6
A	77	40	117	79	57/254	21/57
B	–	82	155	110	96	24/67
C	–	86	213	–	–	29/110
D	127	65/199	131	149	82	93
E	–	71/371	224	188	135	55/152
F	–	163	241	–	–	65/185
G	196	82/341	180	154	146/496	115
H	–	427	257	229	168	76/168
I	–	224/502	309	–	–	299

the different test sections must be given here: in the case of TS3, only one predominant single peak is usually obtained on the spectra, together with smaller peaks at lower frequency. With TS2 and TS6, two significant peaks of similar amplitude are obtained for most of the flow conditions. Data obtained with TS4 and TS5 are not so clear, since several peaks of comparable magnitude often appear on the spectra. Amplitudes of the peaks are usually much lower than in the previous cases, and no frequency can be detected for tests performed at the highest pressure (cases C, F, and I). In the case of TS1, characteristic frequencies can be identified only in cases A, D, G, that is tests performed at the lowest pressure. Figure 7 gives examples of the spectra obtained for each test section, for test case G ($V_{\text{ref}} = 17$ m/s, $\sigma = 0.96$).

Results derived from the FFT analysis of the accelerometer and microphone signals have been compared with the data reported in Table 6. Although the spectra are sometimes different, frequencies identified in Table 6 were systematically obtained with this second analysis. However, note that the peak associated with the cavitation unsteady behavior is not systematically the largest one in the FFT signals.

It was expected that the frequency would increase with flow velocity and with cavitation number, as a small cavity oscillates faster than a big one. This is what is clearly obtained in the present results, for all test sections, as can be checked in Table 6. The calculation of the Strouhal numbers for all cases of data set 1 reveals the occurrence of two distinct unsteady behaviors (Fig. 8):

- A classical value close to 0.2 is obtained with TS3 (the biggest test section) for all flow conditions. This result is in full agreement with previous investigations of cloud cavitation, where a Strouhal number $St \approx 0.3$ is usually reported (Stutz and Reboud 1997; Coutier-Delgosha et al. 2007). Indeed, note that St in the present study is based on V_{ref} the velocity at the Venturi throat, while it is calculated with the velocity upstream from the cavitation area (so for the present geometry, upstream from the convergent) in these former publications.
- On the other hand, a much lower value $St \approx 0.05$ is nearly systematically obtained with TS1, TS4 and TS5, when flow condition leads to unsteady behavior.
- In the tests with TS2 or TS6, frequencies leading to both values of St are most of the time obtained. In TS2, $St \approx 0.05$ is predominant in cases A, B, C, D, F, while $St \approx 0.2$ gives the main peak in cases E, G, H, I. Conversely with TS6, the principal peak in the FFT is obtained for $St \approx 0.2$.

These various behaviors are summarized in Fig. 8, where the Strouhal numbers are indicated for all test cases of data set 1. When two peaks are detected on the FFT, the two associated Strouhal numbers are drawn.

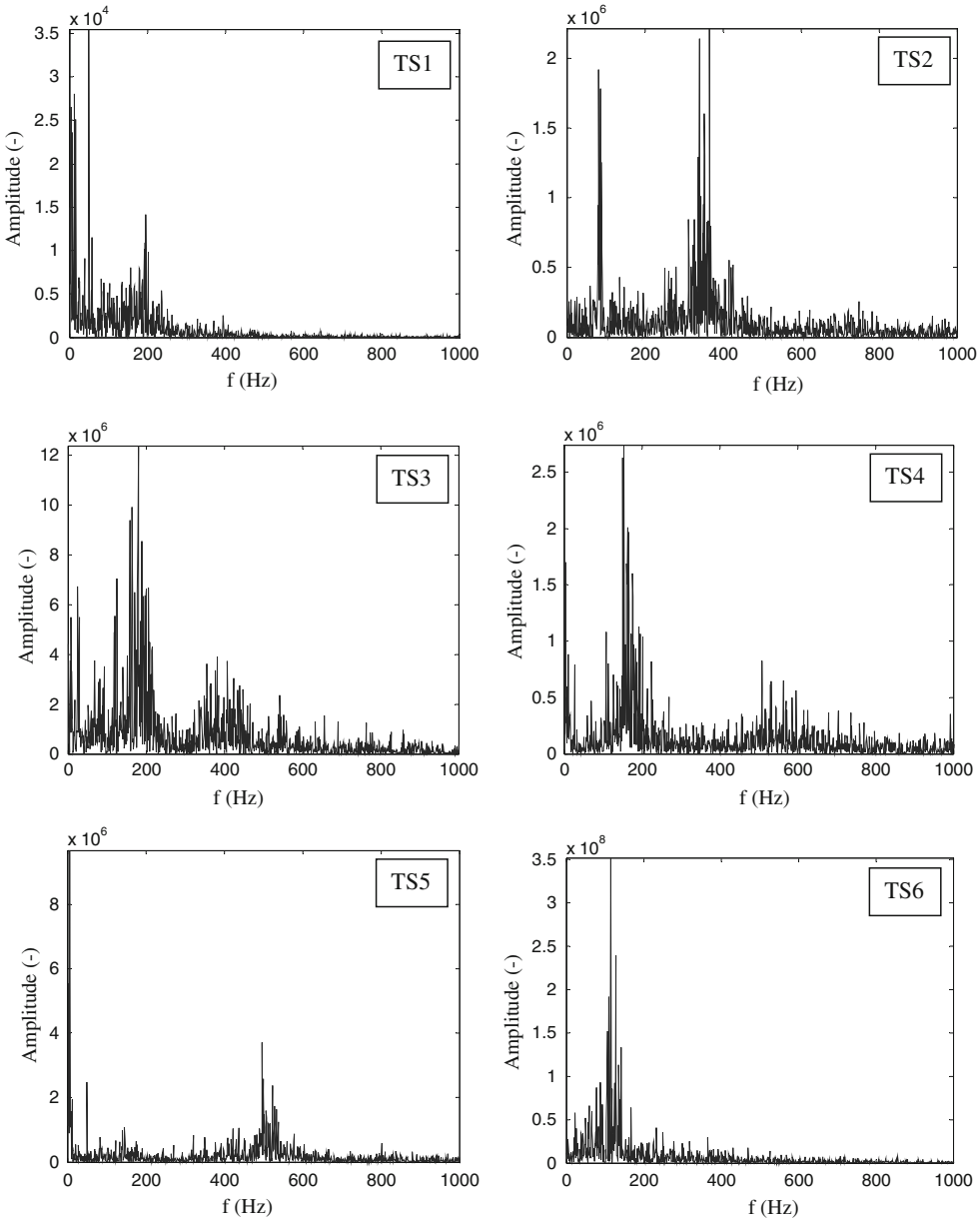

Fig. 7 Typical spectra obtained from local image analysis with the six test sections for test case G ($V_{ref} = 17$ m/s, $\sigma = 0.96$)

These results suggest that two concurrent mechanisms are involved in the unstable behavior of the sheet cavity, with variable influences that depend on the geometry of the test section. Section 3.4 hereafter focuses on this issue.

3.4 Investigation of the unsteady mechanisms

A closer examination of the records is performed in the present section, in order to investigate the physical mechanisms associated with the characteristic frequencies detected previously.

In case of TS1, TS4, and even TS5, results are very clear: for nearly all hydraulic conditions, excepted cases A and G with TS5, only a low Strouhal number close to 0.05 is obtained. These results are associated with behaviors of types 2, 3, or 4, as reported in Table 5. It means that oscillations of sheet cavities (types 3 and 4) are systematically characterized by a low frequency leading to $St \approx 0.05$. When shedding of individual bubbles or small bubble clusters are observed (type 2 in cases A and G with TS5), the frequency is not modified.

In the case of TS3, results are also quite simple: a classical periodical behavior with large-scale shedding is obtained, which leads in nearly all cases to a single frequency that gives $St \approx 0.2$. This frequency in these cases is controlled by the shedding, which have been connected in many previous studies to the re-entrant jet that flows upstream at the same frequency. Only cases A and B seem more complex, as two frequencies are obtained.

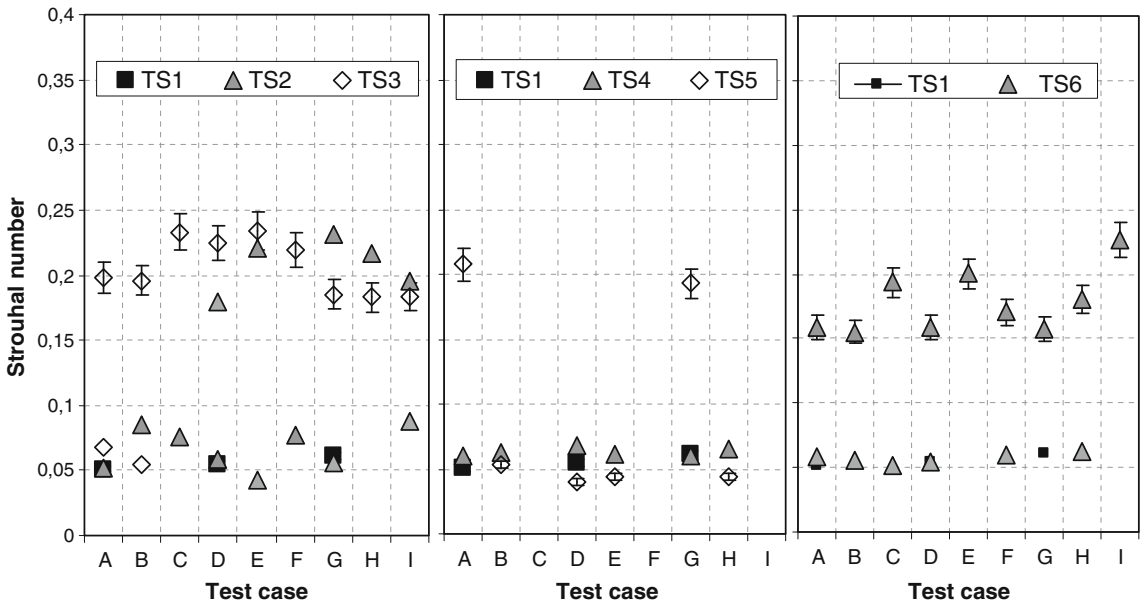

Fig. 8 Strouhal numbers calculated on the basis of the oscillation frequency of the sheet cavity, the velocity at the Venturi throat and the mean length of the sheet cavity

Two coexistent frequencies are also found in most of the cases with TS2 and TS6. This was not expected, since large-scale shedding is visually observed in all cases. High frequency will be denoted f_1 hereafter, and low frequency f_2. It can be observed that the ratio f_1/f_2 is usually close to 3, but it is not constant, so it can be anticipated that phenomena responsible for f_1 and f_2, respectively, are probably not directly connected to each other. To analyze this point, data recorded in case H with TS6 are investigated in more detail. In this cases, $f_1 = 76$ Hz, and $f_2 = 168$ Hz. Note that several peaks of similar magnitude are obtained near f_2. The FFT is calculated for several positions of the window used to select and sum the pixels of the image. Figure 9 shows the results obtained (1) far away downstream (A), (2) inside the cavity at location of the shedding (B), (3) on the way of the re-entrant jet (C), (4) very near from the Venturi throat (D). It can be checked that positions C and D make frequency f_2 preponderant, which shows that the re-entrant jet progression occurs intermittently at frequency f_2. Conversely, both frequencies are detected at position B, and the peak at frequency f_1 becomes the highest at position A, in the wake of the sheet cavity. It suggests that frequency of shedding is complex: although each re-entrant jet occurrence leads to a vapor cloud detachment, only a part of them (about one-third) reaches the left part of the images.

To understand this issue, a portion of the time signal used to obtain the FFT at position B is displayed in Fig. 10. Peaks responsible for frequency f_1 can be clearly distinguished from peaks of lower amplitude that lead to frequency f_2. Images corresponding to the different peaks of large amplitude (A_1–A5) and two smaller intermediate peaks (B_1 and B_2) are displayed in Fig. 10. It can be observed that peaks A_i correspond to large vapor clouds, which are convected far away downstream before collapsing, while peaks B_i usually denote smaller clouds and/or clouds that detach from a smaller sheet cavity and collapse faster. This interpretation results from the analysis of the whole time signal, not only the small part presented in Fig. 10. It suggests that some global fluctuation of the sheet cavity at frequency f_1 is superimposed with the periodical shedding at frequency f_2. This conclusion is confirmed by the study of all test cases recorded with TS6: in all cases, the highest frequency is clearly related to the re-entrant jet and the shedding of vapor cloud, while the low frequency is associated with periodical large-scale oscillations of the sheet cavity. Observation of both phenomena is sometimes complicated, especially if f_2 is not a multiple of f_1. Moreover, for low values of V_{ref}, frequency f_2 is scattered over a larger range of frequencies, since cloud shedding is not so regular. Test case A is representative of such more complex behavior: f_1 equals 21 Hz, f_2 is comprised between 40 and 80 Hz (see Fig. 11a), and although the FFT derived from a window located far away downstream exhibits only frequency f_1 (Fig. 11b), the explanation cannot be found in the examination of the shedding. On the other hand, it can be remarked that the cloud structure downstream from the attached cavity regularly disappears on the images, at frequency f_1. This behavior, which is illustrated by Fig. 11c, may be still due to a global pressure/cavity fluctuation. Such fluctuation could be connected to a system instability driven by the pump or another equipment of the test rig.

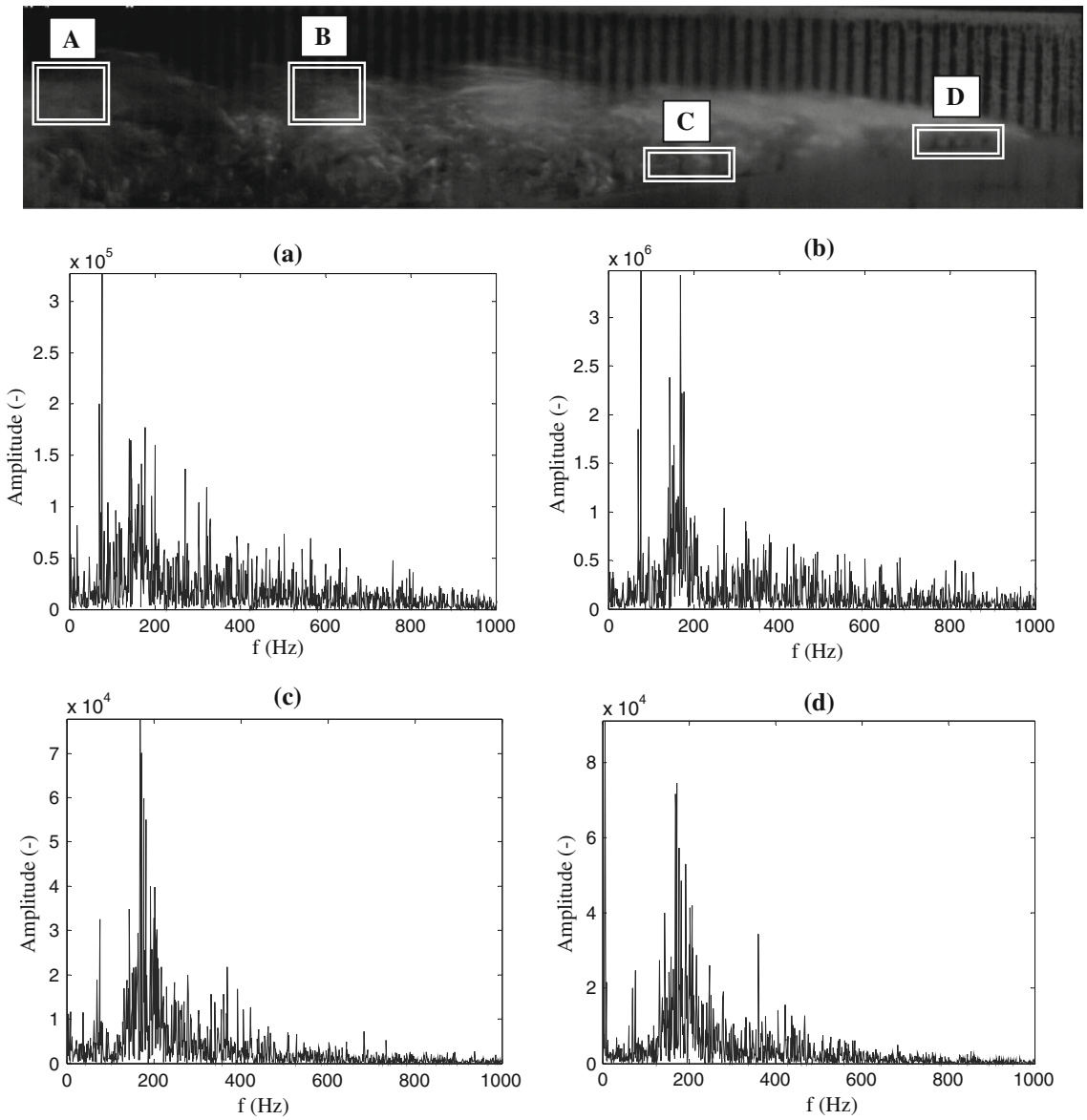

Fig. 9 FFT at different locations of the images (point H of data set 1, TS6) ($V_{ref} = 17$ m/s, $\sigma = 0.98$, $Re = 8.09 \times 10^4$)

However, it can be checked in Table 6 that frequency f_1 varies not only according to the flow velocity but also the cavity size at constant velocity, which suggests that the associated periodical phenomenon is very probably inherent to the cavitation area.

The low-frequency global instability of the sheet cavity observed in nearly all test cases with TS2 and TS6 is consistent with the behavior obtained with test sections TS1, TS4, and TS5, where only this frequency is detected, as previously mentioned. Such oscillation of the cavity was not reported previously at large scale, so new measurements were performed in the scope of the present study by colleagues from DynFluid laboratory (Paris) in the same Venturi-type section of width 120 mm and height 67 mm. These dimensions are still bigger than the one of the original test section in the LEGI laboratory (see Table 1). Flow conditions $V_{ref} = 8$ m/s and $L_{cav} = 11.8$ cm, which are very close to the ones of test case A in data set 1, are considered. A classic unsteady behavior including periodical large vapor shedding is obtained. The FFT signal derived from image analysis in the wake of the sheet cavity is drawn in Fig. 12a. It shows that only frequency $f_2 = 18.5$ Hz, which leads to $St = 0.26$, is obtained. No lower frequency can be detected, as can be checked also on the time signal (Fig. 12b). This result shows that self-oscillation of sheet cavity is not obtained at large scale,

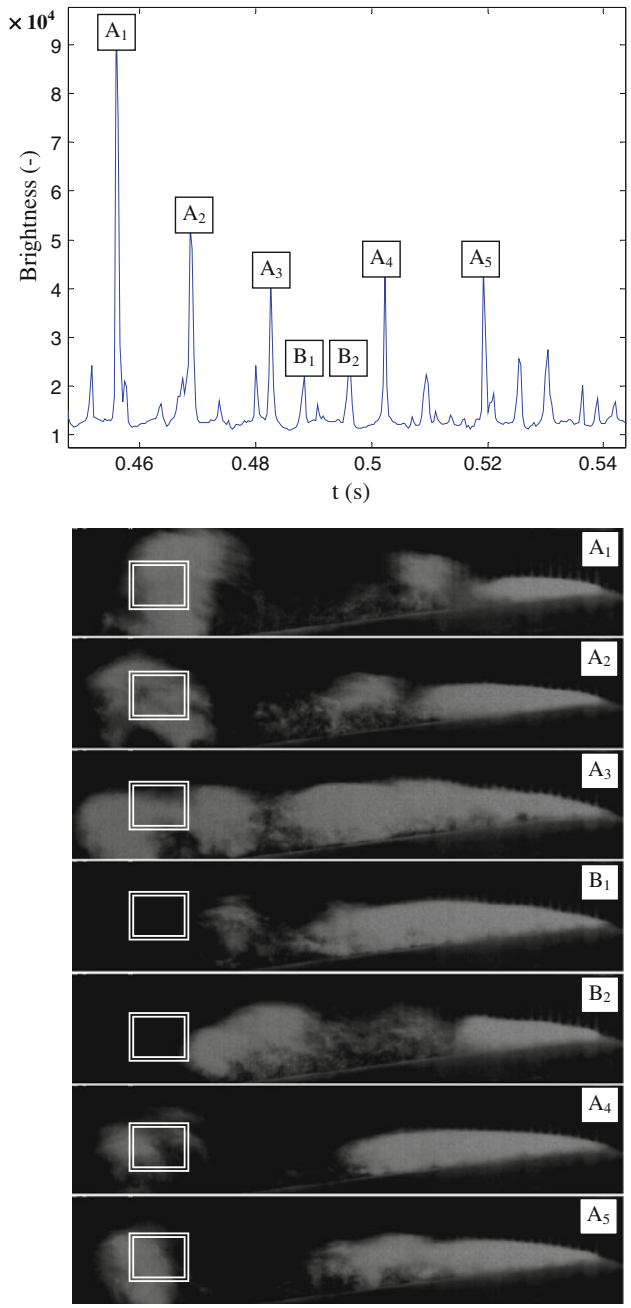

Fig. 10 Further analysis of time signal (point H of data set 1, TS6) (V_{ref} = 17 m/s, σ = 0.98, Re = 8.09 × 10^4)

which suggests that this instability is specific to the small scales studied in the frame of the present work.

3.5 Effect of Reynolds and sheet cavity length

Cases of data set 1 are not in similarity with results at large scale, since the Reynolds number is much lower in the present experiments. In data set 2, the Reynolds number has been increased with TS1 up to 8.9 × 10^4 and with TS3 up to 2.6 × 10^5, for σ = 0.96 (Table 3). These values are of the same order of magnitude as Re = 5.4 × 10^5 obtained in the experiments at large scale in DynFluid.

Results at high velocity are very similar to the one shown previously, as well with TS1 as with TS3: TS1 leads for all velocities to small-scale oscillations of the sheet cavity only, while periodical shedding is obtained with TS3. Figure 13 displays the evolution of the Strouhal number according to V_{ref} in this second configuration: a nearly constant value close to 0.18/0.2 is obtained for all values of V_{ref}, which means that increasing the flow velocity does not modify significantly the cavitating behavior.

Influence of the cavity length on the results has been also investigated in data set 3 by decreasing the cavitation number down to 0.91 (TS1) and 0.94 (TS3) for various Reynolds numbers in the same range as previously for data set 2 (Table 4). In both cases, the non-dimensional mean length of the sheet cavity is substantially increased, compared with the flow conditions of data set 1: L_{cav}/h is close to 4 with TS1 and 3.5 with TS6, whereas it was comprised between 1 and 2.5 in data set 1 (see Fig. 5).

Periodical cloud shedding is still obtained with TS3 for all values of velocity, as expected. It can be checked in Fig. 13 that the Strouhal numbers are remarkably close to the ones obtained in data set 2, which confirms that the unsteady cavitation cycle is almost independent on pressure and velocity, at scale of TS3. Conversely, a clear influence of the cavity length is observed at small scale with TS1: large cavity oscillations including regular shedding are obtained here, while only small-scale irregular oscillations were detected in data sets 1 and 2. Strouhal numbers are very close to 0.2 for all values of flow velocity. Figure 14 displays some successive images of the sheet cavity during one cycle: as can be seen, only the rear part of the cavity is detached and convected downstream, which implies that small dimensions of the test section still influence strongly the cavitation behavior.

3.6 Internal structure of cavitation

In the present section, the modification of the two-phase structure according to the scale is investigated. Figure 15 shows two images of cavitation: on the left obtained with TS1 at cavitation number 0.96 and flow velocity 9 m/s (point A) and on the right in section 3 at the same cavitation number and velocity.

In the small section, the vapor structure consists of finite number of larger individual bubbles. This is especially clear from the light reflection at the front part of the cavity, which is made of a single big bubble. On the other side in the bigger section, the internal structure of the cavity is more homogeneous and made of numerous smaller bubbles.

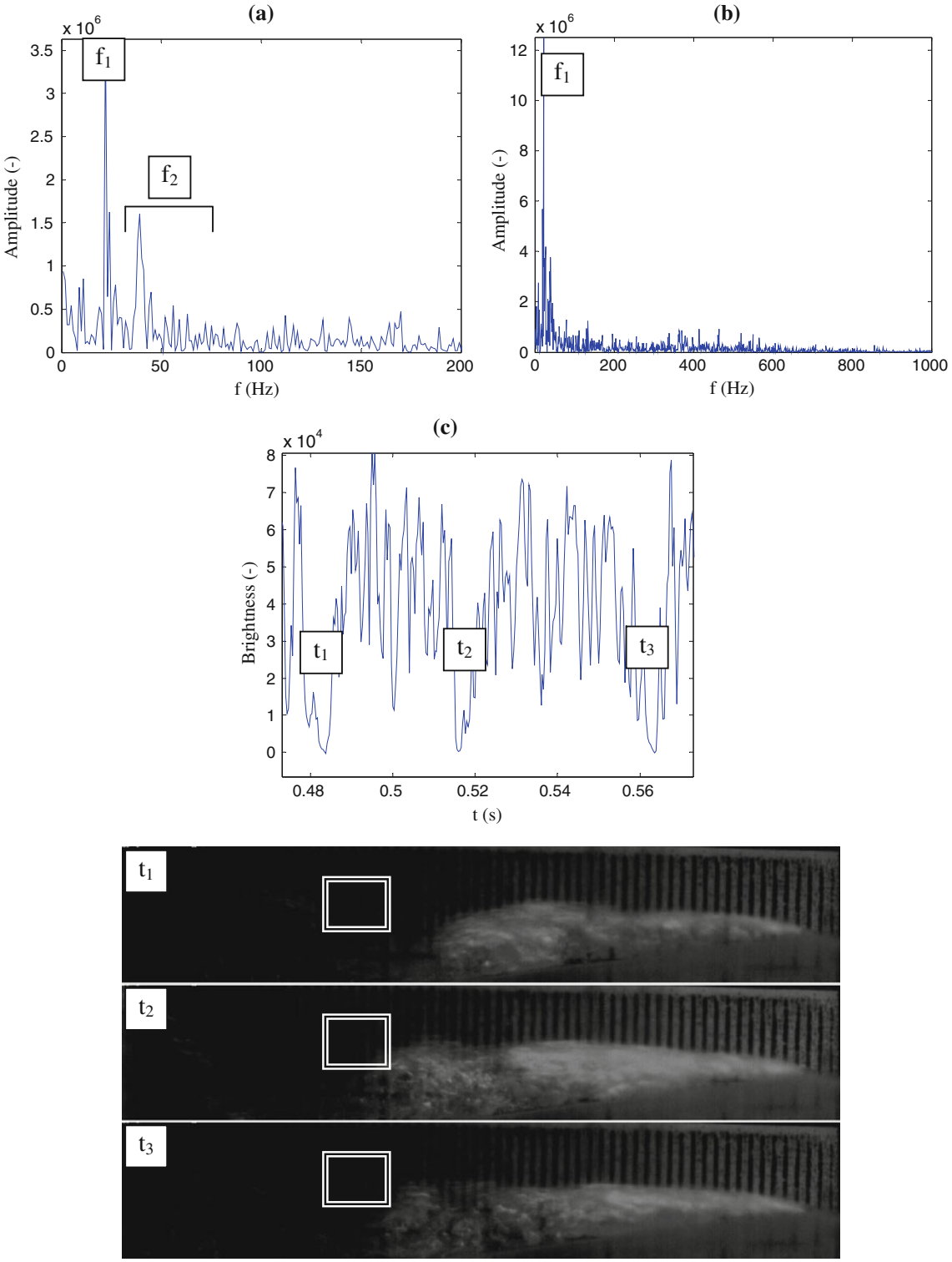

Fig. 11 Analysis of case **a** of data set 1 with TS6 ($V_{ref} = 9$ m/s, $\sigma = 0.96$, $Re = 4.44 \times 10^4$)—the position of the observation window is the same as the window **b** in Fig. 9

Measurements by fast X-ray imaging performed by Vabre et al. (2009) and Coutier-Delgosha et al. (2009) in a Venturi-type section of small dimensions close to the ones of TS1 (height 3.3 mm, width 4 mm) are consistent with these findings. Among other advantages, the X-ray illumination enables to visualize the vapor bubble interfaces by phase contrast imaging. Recorded images reveal that a large deformed vapor bubble forms at the sheet cavity

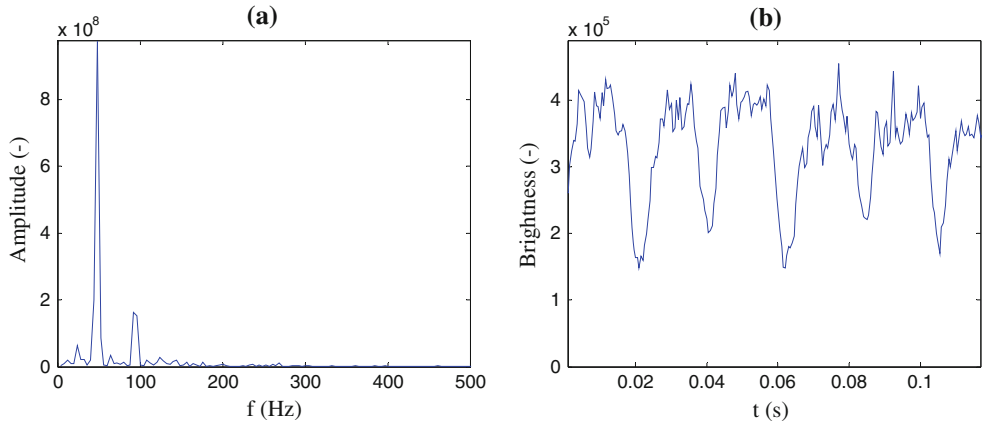

Fig. 12 Results at large scale (data obtained by colleagues of DynFluid Laboratory) ($V_{ref} = 8$ m/s, $L_{cav} = 118$ mm, $Re = 5.4 \times 10^5$)

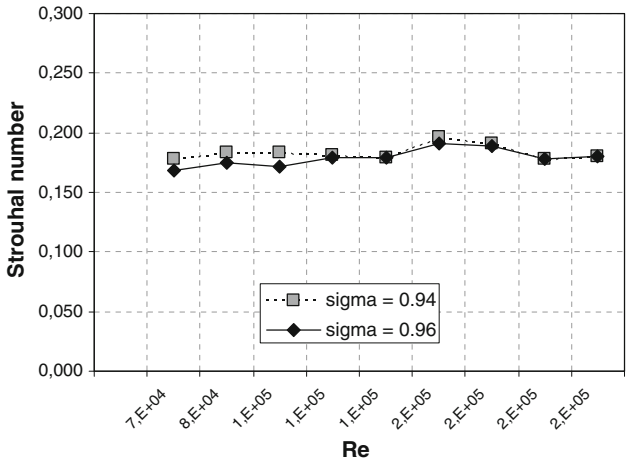

Fig. 13 Influence of Reynolds number and cavity length (data sets 2 and 3)

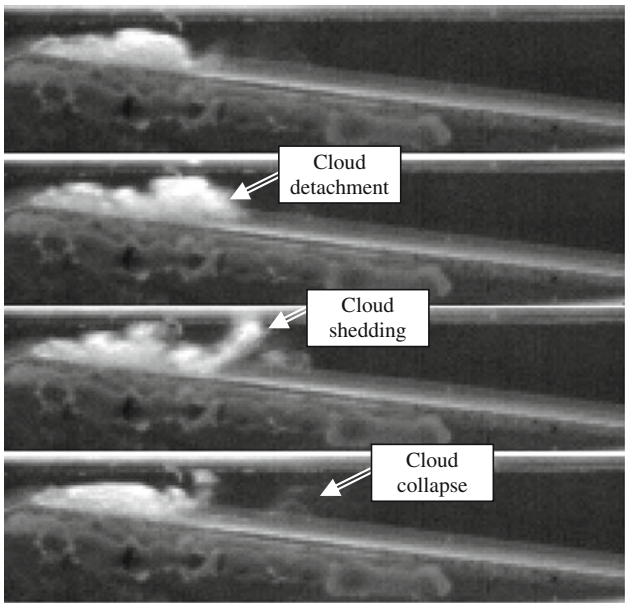

Fig. 14 Sheet cavity behavior in TS1 (data set 3: $\sigma = 0.91$, $V_{ref} = 17.9$ m/s, $Re = 6.05 \times 10^4$)

upstream end, near the throat of the Venturi. For $V_{ref} = 9$ m/s and $L_{cav} \approx 8$ mm (which gives $L_{cav}/h \approx 2.4$ so flow conditions similar to test case A in data set 1). The smaller bubbles downstream are probably just a result of bubble breakup due to decreased surface tension forces. This behavior is not present in bigger geometries at similar conditions. For example, Coutier-Delgosha et al. (2006) showed that larger bubble clusters do form at larger scale, but they are still made of a number of individual bubbles whose size does not vary much inside the attached cavity—like in section 3 (see Fig. 15b).

4 Discussion

In the present section, a physical interpretation of the results shown previously is proposed. At scales used in most of the previous studies of unsteady developed cavitation, each shedding is initiated by the slow growth of the attached part of the cavity. The pressure difference between the inside and the outside of the attached cavity causes the deviation of the flow toward the solid wall in the vicinity of the cavity closure. The flow then separates into i) the outer-flow, which reattaches to the wall and ii) the re-entrant jet, which flows upstream, turns upwards, "cuts" the cavity and consequently causes the cavitation cloud to separate. While the separated cloud flows downstream and collapses in the higher pressure region, the attached cavity begins to grow again and the process is repeated. This behavior is obtained in the present work with the largest test section TS3 (scale 1/4). As explained in Sect. 3.4, it is also partially obtained with test sections of intermediate dimensions, that is TS2 (scale 1/6) and TS6 (large height, small width). Conversely, it is almost never observed with TS1, TS4, and TS5, which are test sections with the smallest height and various widths.

Indeed, since the height of the throat is very small in these three configurations, the re-entrant jet cannot "cut"

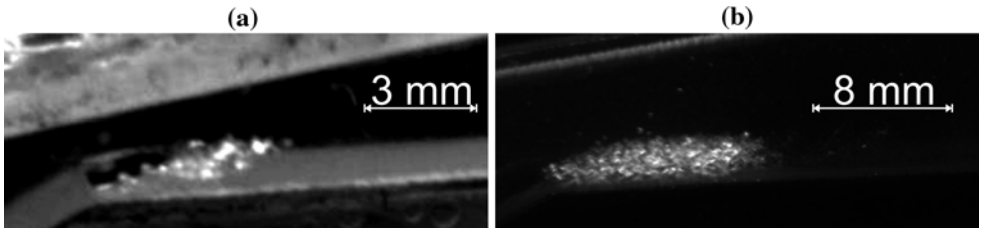

Fig. 15 Structure of the cavity in (a) TS1, (b) TS3 for case A of data set 1 ($\sigma = 0.96$, $V_{ref} = 9$ m/s, $Re = 2.52 \times 10^4$ (TS1) and $Re = 8.71 \times 10^4$ (TS3))

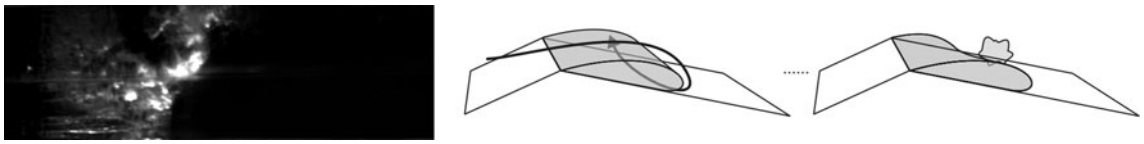

Fig. 16 Cavitation from the top point of view in the wide test section (TS5, point A) ($V_{ref} = 9$ m/s, $\sigma = 0.96$, $Re = 3.48 \times 10^4$)

the cavity. Instead, it looses momentum and flows downstream within the cavity. We suspect that the reason behind this phenomenon is the vicinity of the upper channel wall and its boundary layer—as the jet turns toward it a sort of stagnation point develops inside the cavity and the re-entrant jet is deflected downstream (and possibly also upstream) before it has a chance to cut the cavity in two. Also the ratio between the boundary layer thickness and the height of the throat is larger for smaller test sections. This means that (provided the average flow velocity is the same) the core of the flow needs to move at a higher speed—the re-entrant jet needs more energy to penetrate into the core flow and cut the cavity in two. A similar observation was also made by Callenaere et al. (2001) on a diverging step where they report that thin cavities do not oscillate in length but do exhibit a re-entrant jet behavior. Their interpretation of the phenomenon is that the cloud cavitation requires negligible interaction between cavity and the re-entrant jet, which occurs only when the cavity is thick enough (in the case of thin cavity, the interaction causes the loss of momentum of the jet). Moreover, they report that the re-entrant jet velocity in thin cavities is only about 60 % of its velocity in cloud cavitation regime what could also cause the inability for the jet to cut the sheet cavity in two. Periodical stopping of the re-entrant jet causes the cavity size to oscillate significantly (what was indicated as types 3 and 4 in Table 5). Re-entrant jet existence was confirmed recently in the section of similar size (height 3.3 mm, width 4 mm) used for velocity measurements by fast X-ray imaging (Coutier-Delgosha et al. 2009). Synchrotron X-ray illuminations enabled to obtain the velocity fields in both liquid and vapor phases by techniques derived from PIV (particle image velocimetry). It was shown that a periodical re-entrant jet occurs even in such flow configuration with no shedding.

The difference in the flow dynamics also explains why the frequency of the oscillations is much lower in test cases investigated with TS1, TS4, and TS5 than in other cases ($St \approx 0.05$ instead of 0.2, as detailed in Sect. 3). In the big section flow passes the cavity, turns downstream toward the wall, flows upstream (re-entrant jet), turns upwards, cuts the cavity, meets with the main flow and flows downstream with the separated cavitation cloud. The velocity of this flow over the cavity is somewhat higher than the free stream velocity and can be estimated to $V_{ref}\sqrt{1+\sigma}$ (de Lange and de Bruin 1998). The difference in the small section is that the re-entrant jet stops inside the cavity and does not meet the higher velocity flow above the cavity. Hence, it flows downstream at a much slower speed what prolongs the time of one period of sheet cavity oscillation.

To explain why in the wide sections (TS4 and TS5), cavitation cloud separates from time to time, while in nearly all cases, cavity remains attached, one has to observe the phenomenon from the top point of view. Figure 16 shows on the left an image of cavitation in TS5 (point A of data set 1), and on the right a scheme of the situation. Like in the smallest test section TS1, the re-entrant jet is initiated in the rear part of the cavity. It flows upstream turns upwards but cannot cut the cavity due to the small height of the throat. But the width of the test section is much bigger in TS4 and TS5 than in TS1, so the reverse flow has plenty of space to turn either left or right—toward one of the side walls. The result is similar to the one obtained on hydrofoils with swept leading edge (Laberteaux and Ceccio 2001b; Dular et al. 2007). The re-entrant jet flows toward one of the walls and "cuts" the sheet cavity only in that region. The direction of the jet exiting the attached cavitation area is not normal to the flow above the cavity, but at a sharp angle; hence the separated clouds appear smaller. Analysis of the whole data shows that in TS4 and TS5, vapor clouds are shed only at the end of 25 and 40 % of the cycles, respectively. During other periods, the attached cavity just oscillates without any noticeable vapor detachment.

This also agrees with the findings of Kawanami et al. (1998) who report that for a case of a hydrofoil, the spanwise length of the shed cavities depends on the cord wise length of the sheet cavity. They also report that at a certain ratio between the length of the sheet cavity and the channel width, an irregular break-off pattern or multiple clouds shedding will occur.

An indirect evidence of the modified shedding mechanisms in TS4 and TS5 can be also found in the results obtained with TS6. Indeed, shedding characterized by Strouhal numbers close to the classical value of 0.2 was systematically obtained (see Fig. 8), although the width of the section is only 3.6 mm. It confirms that the complete re-entrant jet mechanism is mainly influenced by the height of the test section, at such small scales. It can be noticed in Fig. 8, however, that the Strouhal numbers obtained with TS6 are slightly lower than the ones measured with TS2 or TS3: the mean value is close to 0.17, whereas it is about 0.2 with these two other test sections, and also at large scale in the experiments performed in DynFluid. Possible errors on frequency and cavity length measurements cannot be responsible for this decrease of the Strouhal numbers (see the levels of uncertainties in Fig. 8). As reported in Sect. 3.4, the unsteady behavior in TS6 is characterized by two complementary mechanisms: one is the re-entrant jet progression and associated shedding at frequency f_2, the second is a global fluctuation of the sheet cavity, which gives peaks at frequency f_1 of similar amplitude. It can be supposed (but not demonstrated) that only a part of the re-entrant jet succeeds in turning upward and cutting the cavity, while a significant part of its momentum is blocked within the cavity, and just contributes to (or even drives) the low-frequency oscillation of the sheet cavity, like in TS1. The reduction of the momentum responsible for vapor cloud detachment may explain the small slow down of the shedding cycle for all flow conditions in TS6.

5 Conclusions

An experimental study was carried out to investigate the influence of the size of the test section on the structure and dynamics of cavitation. Scaling the width, the height or both dimensions of the section enabled investigation of the influence of all parameters. High-speed visualization, accelerometer and microphone measurements were simultaneously used to determine the frequency of cavitation oscillations according to the flow conditions.

It was shown that small scale has a significant influence on cavitation. Especially the height of the test section plays a major role in the dynamics of the re-entrant jet that is responsible for the periodical shedding observed at large scale. Reducing drastically the height down to a few millimeters leads to a strong modification of the shedding process: vapor cloud detachment is completely stopped if width of the test section is also very small, while partial intermittent shedding is still obtained if the width is increased. Such behavior was attributed to the inability of the reverse flow to cut the cavity and provoke its partial detachment. The small height induces a premature stop of the re-entrant jet progression, leading to more or less pronounced low-frequency oscillations of the attached cavity, without any shedding.

At the largest scales studied (about 15 mm in height and/or in width), it was found that this effect, although it does not suppress vapor shedding, leads to the superposition of the shedding with oscillations of the sheet cavity at lower frequency. In some cases (scale 1/6 or big height and small width), the two phenomena lead to frequency peaks of similar amplitude on the FFT signals.

It was also shown that the structure of the vapor/liquid mixture itself changes when the dimensions of the test section are scaled down. In small sections, large stretched bubbles appeared.

The different sets of results and subsequent analysis have revealed that cavitating flows at millimetric scale may behave differently from cavitating flows at usual scale. Unsteady shedding as well as the two-phase flow morphology is both impacted. This suggests that the characteristic size of the vapor bubbles does not change proportionally with the largest scale of the flow. Moreover, some phenomena such as surface tension, which are almost never taken into account at large scale, may play a non-negligible role when most of the vapor bubbles have radius of the order of magnitude of a few hundreds of μm and less.

At last, we also need to discuss the possibility of system instabilities which could significantly influence the cavitation behavior as Franc (2001) and Kawakami et al. (2008) report. The test rig was designed to minimize such effects. The upstream and downstream partially filled water tanks ensure that system pressure oscillations are attenuated. Attenuation is also achieved through long flexible pipes that connect the tanks. The gas content influence should not play a major role as the water was prepared in the exact the same way for every set of experiments. Also the possibility of the influence of the self generation of nuclei by cavitation in the test section is small since the ratio between the water volume and the flow was big (it took about a minute for all the water to circulate and the residence time in the free surface water tanks, where degassing occurs, was relatively long).

Acknowledgments This work was performed in the scope of a position of invited researcher in the LML laboratory awarded by CNRS (Centre National de la Recherche Scientifique) to M. Dular.

The authors also want to thank their colleagues from Arts et Metiers ParisTech/DynFluid Laboratory F. Ravelet, A. Danlos, and F. Bakir for the data measured at large scale. The technical staff of the LML laboratory was much involved in the initial development of the small-scale test facility. The authors wish to thank especially J. Choquet and P. Olivier for their collaboration.

References

Ackeret J (1930) Experimentelle und theoretische Untersuchungen über Hohlraumbildung (Kavitation) im Wasser. Forsch Ingenieurwes 1(2):63–72

Amromin E (2002) Scale effect of cavitation inception on a 2D Eppler hydrofoil. J Fluids Eng 124(1):186–193

Arakeri VH, Acosta AJ (1973) Viscous effects in inception of cavitation on axisymmetric bodies. J Fluids Eng 95(4):519–526

Arndt REA, Song CCS, Kjeldsen M, He J, Keller A (2000) Instability of partial cavitation: a numerical/experimental approach. Proceedings of the 23rd symposium on naval hydrodynamics, office of naval research, Val de Reuil, France, National Academic Press, Washington, DC, pp 599–615

Billet ML, Holl W (1981) Scale effects on various types of limited cavitation. J Fluids Eng 103(3):405–414

Callejon J, Emerson A, Gorshkoff A, Kruppa C, van der Muelen J, Peterson F, Taylor DW, Scherer O, Takahashi H (1978) Report of the cavitation committee. In: Proceedings of 15th international Towing tank conference, Hague, Netherlands

Callenaere M, Franc JP, Michel JM, Riondet M (2001) The cavitation instability induced by the development of a re-entrant jet. J Fluid Mech 444:223–256

Coutier-Delgosha O, Fortes-Patella R, Reboud JL, Stutz B (2005) Test case number 30: unsteady cavitation in a Venturi type section. In: Lemonnier H, Jamet D, Lebaigue O (eds) Validation of advanced computational methods for multiphase flow. Begell House Inc, New York

Coutier-Delgosha O, Stutz B, Vabre A, Legoupil S (2007) Analysis of cavitating flow structure by experimental and numerical investigations. J Fluids Mech 578:171–222

Coutier-Delgosha O, Devillers JF, Pichon T, Vabre A, Woo R, Legoupil S (2006) Internal structure and dynamics of sheet cavitation. Phys Fluids 18. doi:10.1063/1.2149882

Coutier-Delgosha O, Vabre A, Hocevar M, Delion R, Dazin A, Lazaro D, Gmar M, Fezzaa K, Lee WK (2009) Local measurements in cavitating flow by ultra fast x-ray imaging. In: Proceedings of FEDSM2009 2009 ASME fluids engineering division summer meeting, 2–5 Aug 2009, Vail, Colorado, USA

de Lange DF, de Bruin GJ (1998) Sheet cavitation and cloud cavitation, re-entrant jet and three-dimensionality. Appl Sci Res 58:91–114

Dular M, Bachert B, Stoffel B, Sirok B (2004) Relationship between cavitation structures and cavitation damage. Wear 257:1176–1184

Dular M, Bachert R, Schaad C, Stoffel B (2007) Investigation of a re-entrant jet reflection at an inclined cavity closure line. Eur J Mech B Fluids 26(5):688–705

Franc JP (2001) Partial cavity instabilities and re-entrant jet. In: 4th international symposium on cavitation, Pasadena, USA

Furness RA, Hutton SP (1975) Experimental and theoretical studies of two-dimensional fixed-type cavities. J Fluids Eng 97:515–522

Gates EM, Billet ML (1980) Cavitation nuclei and inception. In: IAHR symposium, Tokyo, Japan

Holl JW, Arndt REA, Billet ML (1972) Limited cavitation and the related scale effects problem. In: The second international JSME symposium on fluid machinery and fluidics, Tokyo, Japan

Iwai Y, Li S (2003) Cavitation erosion in waters having different surface tensions. Wear 254:1–9

Kawakami DT, Fuji A, Tsujimoto Y, Arndt REA (2008) An Assessment of the influence of environmental factors on cavitation instabilities. J Fluids Eng 130(031303):1–8

Kawanami Y, Kato H, Yamaguchi H (1998) Three dimensional characteristics of the cavities formed on a two dimensional hydrofoil. In: 3rd international symposium on cavitation, Grenoble, France, pp 191–196

Keller AP (2001) Cavitation scale effects empirically found relations and the correlation of cavitation number and hydrodynamic coefficients. In: CAV 2001: fourth international symposium on cavitation, california institute of technology, Pasadena, CA, USA

Laberteaux KR, Ceccio SL (2001a) Partial cavity flows. Part 1. Cavities forming on test objects without spanwise variation. J Fluid Mech 431:1–41

Laberteaux KR, Ceccio SL (2001b) Partial cavity flows. Part 2. Cavities forming on test objects with spanwise variation. J Fluid Mech 431:43–63

Leroux JB, Coutier-Delgosha O, Astolfi JA (2005) A joint experimental and numerical study of mechanisms associated to instability of partial cavitation on two-dimensional hydrofoil. Phys Fluids 17(5):52101

Lush PA, Peters PI (1982) Visualisation of the cavitating flow in a Venturi type duct using high-speed cine photography. In: Proceedings of IAHR Conference on operating problems of pump stations and power plants, Amsterdam

Ooi KK (1985) Scale effects on cavitation inception in submerged water jets: a new look. J Fluid Mech 151:367–390

Park JT, Cutbirth JM, Brewer WH (2003) In: Proceedings of FEDSM2003 Hydrodynamic performance of the large cavitation channel (LCC), Honolulu, USA, 6–11 July

Pham TM, Larrarte F, Fruman DH (1999) Investigation of unsteady sheet cavitation and cloud cavitation mechanisms. J Fluids Eng 121:289–296

Stutz B, Reboud JL (1997) Experiments on unsteady cavitation. Exp Fluids 23:191–198

Stutz B, Reboud JL (2000) Measurements within unsteady cavitation. Exp Fluids 29:545–552

Vabre A, Gmar M, Lazaro D, Legoupil S, Coutier-Delgosha O, Dazin A, Lee WK, Fezzaa K (2009) Synchrotron ultra-fast X-ray imaging of a cavitating flow in a Venturi profile. Nucl Instrum Methods Phys Res A 607(1):215–217